

CONSTITUTIVE MODEL FOR TIMBER FRACTURE USED FOR FE SIMULATION OF LVL ARCH

ELIŠKA ŠMÍDOVÁ*, PETR KABELE

Czech Technical University in Prague, Faculty of Civil Engineering, Thákurova 7, 166 29 Prague 6, Czech Republic

* corresponding author: eliska.smidova@fsv.cvut.cz

ABSTRACT. Non-linear finite element simulation of four-point bending test of a small-size arch is described in this paper. The arch of 780 mm span is made of Yellow Poplar (*Liriodendron tulipifera*) laminated veneer lumber (LVL) and it is manufactured with a through crack parallel to fibers in the middle of its crown. 2D homogeneous orthotropic constitutive model of tensile and shear fracture in timber that has been recently developed and implemented into ATENA[®] finite element software by the authors is used for the numerical calculation. Both standard and compact tension (CT) test results are used for the material model calibration. Results show that the model successfully reproduces the increasing part of the load-displacement response. Furthermore, the model can capture the most distinctive features of the crack pattern.

KEYWORDS: Timber, 2D constitutive model, orthotropic elasticity, orthotropic Tsai-Hill failure criterion, fixed smeared crack model, traction-separation law, compact tension test.

1. INTRODUCTION

Concerning environmental impact, energy efficiency and handling costs, timber and engineered wood products represent a promising alternative to the most frequently used structural materials such as concrete or masonry. The wood-derived products of laminated veneer lumber (LVL), cross-laminated timber (CLT) or glue-laminated timber (GLT) provide increased strengths and stiffness compared to solid wood.

Timber and its engineered products are typical for orthotropic behavior. Sawn timber has three mutually perpendicular axes in which we distinguish independent mechanical properties: longitudinal (parallel to grain), radial and tangential. Let us note that properties, such as tensile strength and modulus of elasticity, related to the direction parallel with fibers substantially exceed those related to the other directions [1]. Natural variability in material properties of timber has been addressed by some authors [2, 3]. This material feature is often tackled by Weibull strength theory [4].

Exposed to tensile and shear loading, timber exhibits linear elastic behavior up to failure that is followed by brittle fracture. In contrast, compression in timber leads to a ductile response [5]. Various failure criteria have been developed for timber [6, 7] out of which a commonly applied one corresponds to a Tsai-Hill formulation [8].

Being a complex biological structure, timber contains natural imperfections such as knots, pitch pockets, reaction wood or cross grain. Because such inhomogeneities have a negative impact on the mechanical properties, structural timber, especially the engineered one, is usually carefully selected and processed to provide an improved structural behavior [1]. Influence of some of these weaknesses (e.g., distribution of knots

and finger joints) to strength and failure pattern of LVL beams is tackled in [9], among others.

Two-dimensional and three-dimensional phenomenological constitutive models capturing timber behavior under multi-axial stress state are based on elasticity [10], classical plasticity [11], multi-surface plasticity [12], smeared crack concept [5, 13], smeared fictitious reinforcing fibers [14] and interface schemes [15–17].

2. CONSTITUTIVE MODEL

For non-linear finite element simulation of 4PBT of Yellow Poplar (*Liriodendron tulipifera*) laminated veneer lumber (LVL) arch, we use the 2D homogeneous orthotropic constitutive model of tensile and shear fracture in timber modified for available input data. The model has been recently developed and implemented into ATENA[®] finite element software [18] by the authors [13, 19].

2.1. MODEL PROPERTIES

Let us review the properties of the modified constitutive model. It captures:

- material orthotropy for small deformations in both linear and non-linear range
- elastic behavior until the anisotropic failure criterion is fulfilled
- inelastic behavior after failure criterion is satisfied
- post-failure response for cracks along the grain
- unloading/reloading behavior

The post-cracking response is treated by the fixed smeared crack model [20] where Reinhardt-Hordijk function is used [21].

2.2. MODEL COMPONENTS

The properties of the model described in Section 2.1 are implemented in the form of (i) failure criterion and (ii) cohesive law.

2.2.1. FAILURE CRITERION

With regard to available input data from literature, we use the most frequently used failure theory for wood. It was proposed by Norris [8] and it is also referred to as the Tsai-Hill criterion. In a 2D stress state, it has the form of Equation Eq. 1.

$$\left(\frac{\sigma_x}{f_{tx}}\right)^2 - \frac{\sigma_x\sigma_y}{f_{tx}f_{ty}} + \left(\frac{\sigma_y}{f_{ty}}\right)^2 + \left(\frac{\tau_{xy}}{f_s}\right)^2 = 1 \quad (1)$$

2.2.2. COHESIVE LAW

Cohesive (traction-separation) law relates crack surface normal traction t_n to relative crack normal displacement δ_n with respect to normal crack direction (n). The cohesive law is expressed by Eq. 2 as follows:

$$t_n(\delta_n) = \begin{cases} f_{ty} \left(\left(1 + \left(\frac{c_1\delta_n}{\delta_{n,crit}}\right)^3\right) \exp\left(\frac{c_2\delta_n}{\delta_{n,crit}}\right) - \exp(-c_2) \left(1 + c_1^3\right) \frac{\delta_n}{\delta_{n,crit}} \right) & \text{for } \delta_n \in [0, \delta_{n,crit}) \\ 0 & \text{for } \delta_n \geq \delta_{n,crit} \end{cases} \quad (2)$$

3. CALIBRATION OF THE MODEL

The model requires in total ten input parameters. Based on data available in the literature, we obtained material input parameters for Yellow Poplar LVL both directly from standard tests and employing inverse analysis of traction-separation relationship from compact tension (CT) test (Figure 1). Representing first part of input parameters for FE simulation of LVL arch, selected standard tensile and shear experimental results [1, 17] are shown in Table 1. Within experimental test campaign of Yellow Poplar LVL arch available in literature [22], only two load vs. crack mouth opening displacement (CMOD) responses of CT specimens cut from the arch base and three load vs. displacement responses of CT specimens cut from the arch crown were reported. It is important to note, that displacement of the latter curves is not relevant being biased by the stiffness of the load-cell. Thus, we estimated the parameters defining cohesive law in crack-normal direction, i.e. $\delta_{n,crit}$, f_{ty} , c_1 , c_2 , in two steps.

First, for each of two responses of CT specimens from the arch base, we get the average of four traction-separation curves using sequentially linear approach to inverse analysis including multi-pass enhancement [23]. Consequently, we find the best fit of the cohesive law Eq. 2 for the average curve. Similarly, we find the best fit for the average of all eight traction-separation curves. The overview of cohesive law parameters

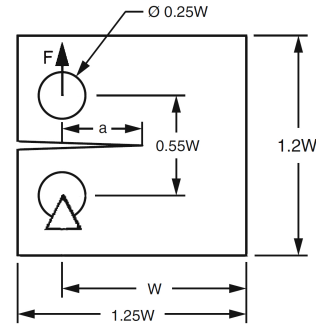


FIGURE 1. Compact tension (CT) test set up: $W = 46$ mm, $a = 20$ mm and thickness is 11 mm.

E_y [MPa]	E_x [MPa]	f_{tx} [MPa]	f_s [MPa]	G_{xy} [MPa]	ν_{xy} [-]
450	14600	110	8.2	899	0.32

TABLE 1. Average values of input data for Yellow Poplar LVL from standard tests [1, 17].

calculated for CT specimens from the arch base is shown in Table 2 together with R^2 statistics that witness a good fit of corresponding responses from finite element simulation and experiment.

Second, for each of three values of maximum load from response of CT specimens sawn from the arch crown, we estimate tensile strength parameter f_{ty} considering remaining parameters of $\{c_1, c_2, \delta_{n,crit}\}$ to be equal to those calculated in step one for CT specimens from arch base. For this purpose, we apply the trial-and-error method to FE inverse analysis. A considerable difference between maximum loads applied to CT specimens cut from the arch base and crown can be observed. Therefore, we use the estimations of cohesive law parameters calculated for the arch crown (Table 3) expecting them to be more representative for FE simulation of the crack pattern spreading across the crown. The responses (load vs. CMOD) and traction-separation relationships (stress vs. COD) from (i) experiments, (ii) sequentially linear or (iii) trial-and-error approach to inverse analysis are displayed in Figure 2 and Figure 3, respectively.

4. FE SIMULATION OF 4PBT OF THE ARCH

The subject of the FE simulation is a four-point bending test (4PBT) of Yellow Poplar LVL arch with a through pre-crack parallel with grain in the middle of its crown [22, 24]. Teflon paper was placed between two laminations preventing them from being glued. The arch has the span of 780 mm, cross-section height and width of 57 mm and 25 mm, respectively, and lamina thickness of 3.2 mm. The overall test setup is depicted in Figure 4.

We generated regular 2D FE mesh composed of approx. 3.2 mm by 3.2 mm quadrilaterals aligned with

Response	$\delta_{n,crit}$ [mm]	f_{ty} [MPa]	c_1 [-]	c_2 [-]	R^2 [-]
max	1.41	15.90	4.10	7.90	0.93
avg	1.07	14.00	4.10	8.60	—
min	0.57	14.00	4.10	10.00	0.96

TABLE 2. Parameters of cohesive law calculated by sequentially linear approach to inverse analysis [23] of load vs. CMOD responses of CT specimens cut from arch base.

$\{\delta_{n,crit}, c_1, c_2\}$ {[mm], [-], [-]}	f_{ty}^{max} [MPa]	f_{ty}^{avg} [MPa]	f_{ty}^{min} [MPa]
{1.41, 4.10, 7.90}	2.60(#1)	2.10(#2)	1.60
{1.07, 4.10, 8.60}	2.90(#3)	2.30(#4)	1.80
{0.57, 4.10, 10.00}	3.90	3.00	2.30

TABLE 3. Parameters of cohesive law estimated by trial-and-error approach to inverse analysis of max. load responses of CT specimens cut from arch crown.

the arch outline and lamina. We assigned fiber orientation to each FE as an input material property. As the proposed material model treats post-cracking behavior by the smeared crack approach, we modeled the pre-crack as a missing row of FE elements. Let us note, that in this way we get the same results as for the pre-crack modeled as a row of FEs with an unloaded smeared crack at the beginning of a numerical simulation. We ran FE simulations of LVL arch for each of 9 estimates of input parameters defining the traction-separation relationship for the arch crown Table 3.

5. RESULTS AND DISCUSSION

We present four most relevant results are presented in Figure 5 in the form of load vs. midspan deflection. Out of them, we calculated the best response for Sim. (#1) (i.e., maximum estimated critical crack opening displacement $\delta_{n,crit} = 1.41$ mm and tensile strength $f_{ty}^{max} = 2.6$ MPa). Regarding significant variability of timber material parameters, the results show that the model can reproduce the increasing part of the load-displacement response well. In order to obtain statistically more relevant results, an experimental campaign containing numerous specimens for each type of test needs to be conducted.

Comparison of crack pattern across arch crown from experiment (Figure 6) and FE simulation (Figure 7) shows that the material model can capture both the crack propagation from the pre-crack tips (primary crack) and crack initiation of the crack below the pre-crack (secondary crack). However, the model neglects initiation of the crack above the pre-crack (tertiary crack). The short crack spacing of only twice the lamina thickness between primary and tertiary crack can cause that stored energy is released by opening

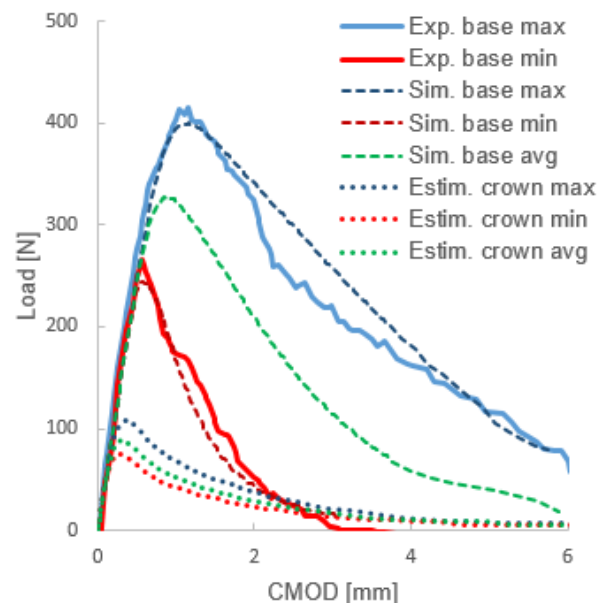


FIGURE 2. Load vs. CMOD responses of CT specimens cut from arch base and crown: (i) experimental (Exp.), (ii) numerically simulated by means of sequentially linear approach to inverse analysis (Sim.) and (iii) estimated by trial-and-error approach to inverse analysis (Estim.).

and spreading of the primary crack instead of the adjacent tertiary crack initiation and growth.

In the end, we can compare the results for Yellow Poplar LVL arch from smeared crack model to the results calculated by interface scheme [22, 24]. To this end, let us briefly describe the latter approach first. Interface elements were placed between the lamina and the initial crack was modeled as a gap of finite length separating the arch layers. Interface behavior was governed by (i) modulus of elasticity and (ii) maximum tensile strength, both in the direction perpendicular to fibers, and (iii) fracture toughness acquired from compact tension specimens cut from arch crown [16]. The response obtained by the interface scheme is shown in Figure 5 as Sim. Interf. This curve represents a weak reproduction of the response compared to Sim. (#1) to Sim. (#4). On the other hand, the interface approach can capture both the primary crack spreading and the secondary crack initiation and growth. Discrepancies between the two approaches can be attributed to:

- (1.) significant variability of timber material parameters that needs to be handled appropriately.
- (2.) specific acquisition of the most relevant input parameters that control the crack initiation and post-cracking behavior.

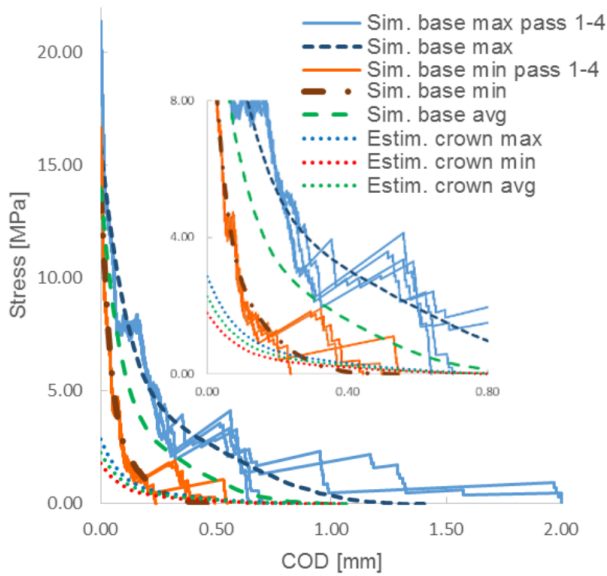


FIGURE 3. Traction-separation relationships (stress vs. COD) of CT specimens cut from arch base and crown: (i) experimental (Exp.), (ii) numerically simulated by means of sequentially linear approach to inverse analysis (Sim.) and (iii) estimated by trial-and-error approach to inverse analysis (Estim.).

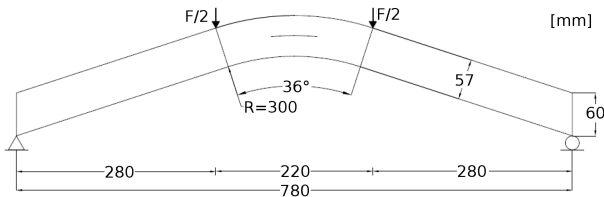


FIGURE 4. Scheme of 4PBT of Yellow Poplar LVL arch with a through pre-crack in its crown.

6. CONCLUSION

We used 2D homogeneous orthotropic constitutive model of tensile and shear fracture in timber for FE simulation of small-size Yellow Poplar LVL arch subjected to four-point bending. We presented the main features of the model. Input data were obtained both (i) directly from standard tensile and shear tests and (ii) by applying inverse analysis to compact tension (CT) test results for Yellow Poplar laminated veneer lumber (LVL). For the limited availability of relevant experimental data from CT test results, we calculated the estimation of parameters that define traction-separation relation.

Numerical simulations of Yellow Poplar LVL arch confirm that the applied constitutive model can capture both the increasing part of the load-displacement response and pre-crack spreading together with the initiation of a secondary crack. We compared the results obtained by utilizing the proposed model to those calculated by interface approach. Both models can predict primary and secondary crack initiation

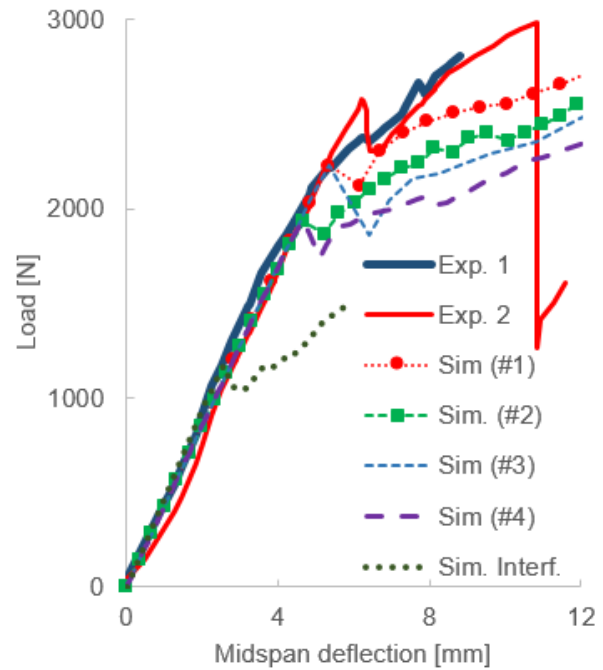


FIGURE 5. Load vs. midspan deflection response of 4PBT of LVL arch obtained from experiments (Exp.) and FE simulations (Sim.).

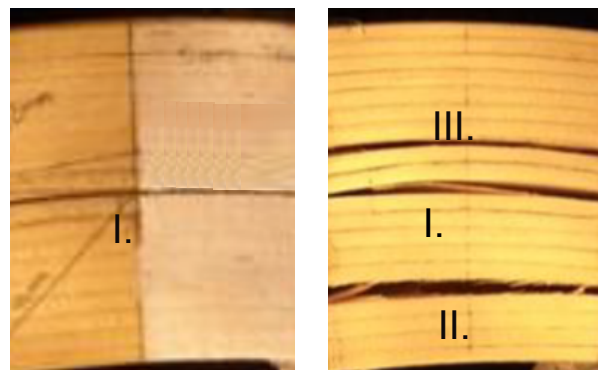


FIGURE 6. Arch crown cracking (primary I., secondary II. and tertiary III.) during experiment at two load levels.

and development well. On the other hand, the interface model yields a weak load vs. midspan deflection response. Considerable variability of timber material characteristics requires both statistically significant results for each type of experiment and an appropriate statistical approach to obtain relevant results from numerical models.

LIST OF SYMBOLS

- c_1, c_2 Material parameters controlling the shape of the softening curve [-]
- δ_n Crack opening displacement [mm]
- $\delta_{n,crit}$ Critical value of crack opening displacement [mm]
- E_x Modulus of elasticity along the grain [MPa]

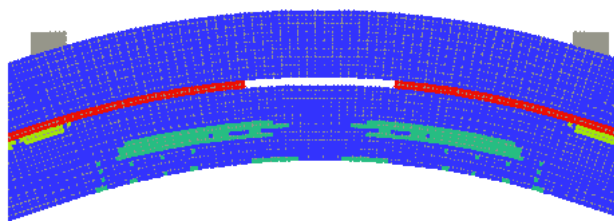


FIGURE 7. Arch crown cracking in FE simulation: primary and secondary crack.

E_y	Modulus of elasticity across the grain [MPa]
f_{tx}	Tensile strength parallel with grain [MPa]
f_{ty}	Tensile strength perpendicular to grain [MPa]
f_s	Shear strength [MPa]
G_{xy}	Shear modulus [MPa]
ν_{xy}	Poisson's ratio [-]
R^2	Coefficient of determination [-]
σ_x	Normal stress parallel with grain [MPa]
σ_y	Normal stress perpendicular to grain [MPa]
τ_{xy}	Shear stress [MPa]

ACKNOWLEDGEMENTS

The support by the GAČR grant No. 18-05791S is gratefully acknowledged.

REFERENCES

- [1] *Wood handbook - Wood as an engineering material*. Forest Product Laboratory, 2010.
- [2] T. Tannert, T. Vallee, S. Franke, P. Quenneville. Comparison of test methods to determine Weibull parameters for wood. *World* **15**:19, 2012.
- [3] L. Melzerova, M. Sejnoha, P. Klapalek. Bending Tests and Simulations of GLT Beams. *Applied Mechanics and Materials* **611**:54–59, 2014. DOI:10.4028/www.scientific.net/AMM.611.54.
- [4] W. Weibull. A statistical theory of strength of materials. In *Proceedings of the Royal Swedish Institute*. 1939.
- [5] S. Holmberg, K. Persson, H. Petersson. Nonlinear mechanical behaviour and analysis of wood and fibre materials. *Computers & structures* **72**(4):459–480, 1999.
- [6] B. Kasal, R. J. Leichti. State of the art in multiaxial phenomenological failure criteria for wood members. *Progress in Structural Engineering and Materials* **7**(1):3–13, 2005. DOI:10.1002/pse.185.
- [7] E. Smidova, P. Kabele. Comparison of failure criteria for wood in tensile-shear stress state. *Acta Polytechnica CTU Proceedings* **13**:115, 2017. DOI:10.14311/APP.2017.13.0115.
- [8] C. B. Norris. Strength of orthotropic materials subjected to combined stresses, 1962.
- [9] L. Melzerova, M. Sejnoha. Influence of distribution of finger joints and timber flaws on the damage evolution of laminated glued timber beams during four point bending. In *WCTE 2016*. Vienna, Austria, 2016.
- [10] N. Khorsandnia, H. R. Valipour, K. Crews. Nonlinear finite element analysis of timber beams and joints using the layered approach and hypoelastic constitutive law. *Engineering Structures* **46**:606–614, 2013. DOI:10.1016/j.engstruct.2012.08.017.
- [11] B.-H. Xu, A. Bouchair, M. Taazount, P. Racher. Numerical simulation of embedding strength of glued laminated timber for dowel-type fasteners. *Journal of Wood Science* **59**(1):17–23, 2013. DOI:10.1007/s10086-012-1296-0.
- [12] P. Mackenzie-Helnwein, J. Eberhardsteiner, H. A. Mang. A multi-surface plasticity model for clear wood and its application to the finite element analysis of structural details. *Computational Mechanics* **31**(1-2):204–218, 2003. DOI:10.1007/s00466-003-0423-6.
- [13] E. Smidova, P. Kabele. Constitutive Model for Timber Fracture under Tensile and Shear Loads. *Applied Mechanics and Materials* **784**:137–144, 2015. DOI:10.4028/www.scientific.net/AMM.784.137.
- [14] H. R. Valipour, K. Crews. Efficient finite element modelling of timber beams strengthened with bonded fibre reinforced polymers. *Construction and Building Materials* **25**(8):3291–3300, 2011. DOI:10.1016/j.conbuildmat.2011.03.017.
- [15] X. P. Xu, A. Needleman. Continuum Modelling of Interfacial Decohesion. *Solid State Phenomena* **35-36**:287–302, 1993. DOI:10.4028/www.scientific.net/SSP.35-36.287.
- [16] X.-P. Xu, A. Needleman. Numerical simulations of fast crack growth in brittle solids. *Journal of the Mechanics and Physics of Solids* **42**(9):1397–1434, 1994. DOI:10.1016/0022-5096(94)90003-5.
- [17] B. Kasal, R. Blass. Experimental and analytical investigation of crack development in composite reinforced laminated arch. *Materials and Structures* **46**(1-2):173–180, 2013. DOI:10.1617/s11527-012-9892-4.
- [18] J. Cervenka, L. Jendele, V. Cervenka. Atena program documentation, part 1, Theory, 2008.
- [19] E. Bartunkova. *Constitutive Model of Timber*. Ph.D. thesis, Czech Technical University in Prague, 2013.
- [20] A. Hillerborg, M. ModeÅr, P.-E. Petersson. Analysis of Crack Formation and Crack Growth in Concrete by Means of Fracture Mechanics and Finite Elements. *Cement and Concrete Research* **6**(6):773–782, 1976.
- [21] H. Reinhardt, H. Cornelissen, D. Hordijk. Tensile Tests and Failure Analysis of Concrete. *Journal of Structural Engineering* **112**(11):2462–2477, 1986.
- [22] R. A. Blass. *Laminated Wooden Arches Reinforced with Glass Fiber Rods*. Ph.D. thesis, The Pennsylvania State University, 2011.
- [23] J. Vorel, P. Kabele. Inverse analysis of traction-separation relationship based on sequentially linear approach. *arXiv:180208040 [cs]* 2018. ArXiv: 1802.08040.
- [24] B. Kasal, R. Blass. Experimental and analytical investigation of crack development in composite reinforced laminated arch. *Materials and Structures* **46**(1-2):173–180, 2013. DOI:10.1617/s11527-012-9892-4.